Coastal Engineering Journal

ANALYSIS OF DIRECTIONAL WAVE SPECTRUM IN SHALLOW WATER AREA USING VIDEO IMAGES DATA

MUHAMMAD ZIKRA *

Department of Maritime Engineering, Kyushu University
744 Motooka, Nishiku, Fukuoka City, 819-0395, Japan
zikra@civil.kyushu-u.ac.id

NORIAKI HASHIMOTO†, MASARU YAMASHIRO‡ and MASAKI YOKOTA§

Department of Urban and Environmental Engineering, Kyushu University
744 Motooka, Nishiku, Fukuoka City, 819-0395, Japan
† *hashimoto-n@civil.kyushu-u.ac.jp*
‡ *yamashiro@civil.kyushu-u.ac.id*
§ *yokota.masaki.426@m.kyushu-u.ac.jp*

KOJIRO SUZUKI

Marine Environmental Information Group, Port and Airport Research Institute
Ministry of Transport, 3-1-1 Nagase, Yokosuka 239, Japan
suzuki_k@pari.go.jp

Received (6 February 2012)
Revised (5 July 2012)

In the present study, a technique for analyzing the directional wave spectrum in shallow water area using video image sequences is presented. The video images data is obtained and collected by single digital video camera. The technique was based on time series of the pixel brightness on video images. The pixel can be treated as a fixed instruments through use of the rectification process. The Extended Maximum Likelihood Method and the Bayesian Directional Method were used to estimate directional wave spectrum using two different configurations of arrays from pixel brightness on video images. The study was examined using video images data at HORS pier on Hasaki beach, Japan. The result indicated that video images data could be used to estimated surface wave spectra in very shallow water area.

Keywords: Directional wave spectrum; pixel brightness; shallow water; video images

1. Introduction

Determination of wave parameters through measurement of ocean surface waves is very important for variety of coastal and marine engineers. The measurement of wave

*Department of Ocean Engineering, *Sepuluh Nopember* Institute of Technology (ITS), Gedung W Kampus ITS Keputih Sukolilo, Surabaya 60111, Indonesia. (Corresponding author)

parameters, such as wave period, wave height and wave direction in shallow water area is the major factor for planning and designing process of harbors, waterways, coastal protection measures and other coastal works. Commonly, information on wave conditions is provided by the measurement of water surface profile which is conducted by in-situ devices such as wave gauges or pressure sensors. Often several in-situ devices are needed to observe the spatial shape pattern in specific location to obtain higher accuracy on wave information. Such kinds of extensive measurements are rather expensive and difficult to maintain.

In recent decades, there has been significant interest in applying the measurement technique of remote sensing such radar or satellite images for the study of wave characteristics. For example wave measurements using satellite-based [e.g., Krogstad and Barstow, 1999], measuring wave spectra with HF Radar [e.g., Hashimoto and Tokuda, 1999], or observation of wave spectra from X-Band radar [e.g., Hasan and Takewaka, 2007; Izquierdo *et al.*, 2005] and etc. These kinds of remote sensing of the water surface elevation could provide some wave data in complementing in situ measurement. If we compare with traditional method, these techniques could provide large scale synoptic information on wave characteristic for coastal areas which can be obtained simultaneously. Furthermore, the inventions of new digital technology of images from video camera system can provide synoptic information on wave parameters in coastal area [Holman and Stanley, 2007]. Since 1980, the capability of video remote sensing techniques have been used and developed into a very useful tool for monitoring coastal changes in the nearshore environment area [Aarninkhof and Holman, 1999]. These capabilities include to study sand bar morphology [Lippman and Holman , 1989], foreshore beach slope [Plant and Holman , 1997], wave runup [Holland and Holman , 1997; Holland *et al.*, 1997], to study wave phase or wavenumber to estimate bathymetry [Stockdon and Holman , 2000; Plant *et al.*, 2007], or for coastal management study [Davidson *et al.*, 2007] and etc.

The basic idea of the remote sensing of video camera is to take a snapshot image of the instantaneous wave pattern in coastal area with assumption that the image brightness at each pixel of the snapshot images can be considered proportional to the intensities of the light reflected from the water surface. Since these successive snapshot images data were collected at a specific period, temporal changes of the wave field can be studied [Chou *et al.*, 2004]. After we have successfully extracted wave number components and derived bathymetry in shallow water area with video images data from Hasaki beach in Japan [Zikra *et al.*, 2010], the applicability of video images from Hasaki beach have to be investigated further. Previous study [Zikra *et al.*, 2011] showed that the time series of pixel brightness on video images at Hasaki site containing information about the energy distribution of the wave field.

Therefore, the main objective of this paper was to present a technique to analyze directional wave spectrum in very shallow water area from pixel brightness on video images data. Estimation of directional wave spectrum will be based on the Extended Maximum Likelihood Method as introduced by Isobe [1984] and the

Bayesian Directional Method (BDM) as proposed by Hashimoto [1987]. In order to obtained detailed directional information, two design arrays were used in such a way to be able to improve the estimation of directional spectrum.

The form of this paper is as follows. A brief review of the mathematical definitions commonly used to describe the directional wave spectrum is given in section 2. The descriptions of study site and the information on wave data are described in section 3. Digital image processing and data analysis are then given in section 4. Discussions on the results are given in section 5, followed by the conclusions in section 6.

2. Basic Theory

2.1. *Directional Wave Spectrum Estimation*

The wave spectrum is normally expressed as the product of the frequency spectrum $S(f)$ and directional spreading function $G(\theta, f)$ as follows:

$$S(f,\theta) = S(f)G(\theta, f)\,. \tag{1}$$

The function $S(f,\theta)$ is called the directional wave spectrum, which is non-negative value and should satisfy the relation

$$\int_0^{2\pi} S(f,\theta)d\theta = S(f)\,. \tag{2}$$

substitution of Eq. 1 into Eq. 2 subsequently removes $S(f)$, yielding

$$\int_0^{2\pi} G(\theta, f)d\theta = 1\,. \tag{3}$$

In advance, the estimation of the directional spectrum can be measured with different measured wave properties such surface profile, surface slope, water particle velocity or pressure fluctuation. The analysis methods for these measurements are all based on the relationship between the directional wave spectrum and the cross-power spectrum.

As introduced by Isobe [1984], the general relationship between the cross-power spectrum for a pair of wave properties and the wavenumber-frequency spectrum shows that the Fourier transformation of the product of the wavenumber-frequency spectrum and the transfer functions of the respective wave properties is equal to the cross-power spectrum, being expressed as

$$\Phi_{mn}(\omega) = \int_{\boldsymbol{k}} H_m(\boldsymbol{k},\omega)H_n^*(\boldsymbol{k},\omega)\exp\left\{-i\boldsymbol{k}(x_n - x_m)\right\} S(\boldsymbol{k},\omega)d\boldsymbol{k}\,. \tag{4}$$

where $\Phi_{mn}(\omega)$ is the cross-power spectrum between the m- and n-th wave properties, ω is the angular frequency, $\boldsymbol{k}$ is the wavenumber vector, H_n is the transfer function from the water surface elevation to the m-th wave property, i is the imaginary unit, and the respective location vector of the probe for the m- and n-th wave property, the wavenumber-frequency spectrum, and * the complex conjugate.

The wavenumber $\boldsymbol{k}$ is related to the frequency f by the following dispersion relationship:

$$\omega^2 = (2\pi f)^2 = g\boldsymbol{k}\tanh \boldsymbol{k}d\,. \tag{5}$$

where g is the gravitational acceleration and d water depth.

Thus from Eq. (5), $S(\boldsymbol{k},\omega)$ can be expressed as a function of f and the wave propagation direction θ, allowing Eq. (4) to be rewritten as

$$\begin{aligned}\Phi_{mn} = \int_0^{2\pi} & H_m(f,\theta)H_n^*(f,\theta)[\cos \boldsymbol{k}(x_{mn}\cos\theta + y_{mn}\sin\theta) \\ & -i\sin \boldsymbol{k}(x_{mn}\cos\theta + y_{mn}\sin\theta)]S(f,\theta)d\theta.\end{aligned} \tag{6}$$

where $x_{mn} = x_n - x_m$ and $y_{mn} = y_n - y_m$ denote the distance vector from measurement point m to n, and $S(f,\theta)$ is the directional wave spectrum of interest.

Regarding the transfer function $H_m(f,\theta)$ in Eq. (6), it is commonly expressed as

$$H_m(f,\theta) = h_m(f)\cos^{\alpha_m}\theta\ \sin^{\beta_m}\theta\,. \tag{7}$$

where $h_m(f)$ and parameters α_m and β_m are derived from linear wave theory, being specified for each measured quantity as summarized in Table 1 (see Hashimoto [1987]).

When $S(\boldsymbol{k},\omega)$ or $S(f,\theta)$ are non-negative functions, then they are termed as the directional spectrum of interest according to the fundamental equations for estimating the directional spectrum based on various simultaneously measured wave properties (Eqs. (4) or (6))

2.2. *Extended Maximum Likelihood Method (EMLM)*

Isobe et al. (1984) proposed the Extended Maximum Likelihood Method (EMLM) to estimate the directional wave spectrum based on various kinds or combination of wave properties. In this method, the directional spectrum is first assumed as a linear summation of the respective cross-power spectra obtained from the arbitrarily measured wave properties, that is,

$$\widehat{S}(\boldsymbol{k},\omega) = \sum_m \sum_n \alpha_{mn}(\boldsymbol{k})\Phi_{mn}(\omega)\,. \tag{8}$$

where $\alpha_{mn}(\boldsymbol{k})$ are coefficients.

Substitution of Eq. (14) into (1) yields

$$\widehat{S}(\boldsymbol{k},\omega) = \int_{\boldsymbol{k}'} S(\boldsymbol{k}',\omega)w(\boldsymbol{k},\boldsymbol{k}')d\boldsymbol{k}'\,. \tag{9}$$

where

$$w(\boldsymbol{k},\boldsymbol{k}') = \sum_m \sum_n \alpha_{mn}(\boldsymbol{k})H_m^*(\boldsymbol{k}',\omega)H_n(\boldsymbol{k}',\omega)\exp\left\{-i\boldsymbol{k}'(x_n - x_m)\right\}\,. \tag{10}$$

Equation (15) indicates that a convolution of the true directional spectrum $S(\boldsymbol{k},\omega)$ and the window function $w(\boldsymbol{k},\boldsymbol{k}')$ is the estimate of the directional spectrum $\widehat{S}(\boldsymbol{k},\omega)$. Therefore, as $w(\boldsymbol{k},\boldsymbol{k}')$ approaches the Delta function , the estimate of $\widehat{S}(\boldsymbol{k},\omega)$ approaches the true directional spectrum $S(\boldsymbol{k},\omega)$. After manipulation, Isobe et al. proposed the following formula for estimating the directional spectrum:

$$\widehat{S}(\boldsymbol{k},\omega) = \frac{\kappa}{\sum_m \sum_n \Phi_{mn}^{(-1)}(\omega) H_m^*(\boldsymbol{k},\omega) H_n(\boldsymbol{k},\omega) \exp\{i\boldsymbol{k}(x_n - x_m)\}} \tag{11}$$

where $\Phi_{mn}^{(-1)}(\omega)$ is the mn element of the inverse matrix $\Phi_{mn}^{(-1)}(\omega)$ and κ is a proportionality constant ensuring $\widehat{S}(\boldsymbol{k},\omega)$ satisfies Eq. (5).

2.3. *Bayesian Directional Method (BDM)*

The second method is the Bayesian Directional Method (BDM), introduced by Hashimoto [1987]. Generally, the BDM provides the highest resolution in estimating the directional wave spectrum. The estimation of a directional wave spectrum can be considered as a regression analysis to find the most suitable model from limited data. The directional spreading function is expressed as a piecewise constant function over each segment of the directional range from 0 to 2 π. It is defined by a series of k values x_k.

$$ln[G(\theta_k)] = x_k(f), (k = 1, ..., K)\,. \tag{12}$$

$$G(\theta, f) \approx \sum_{k=1}^{K} \exp\{x_k(f)\}\, I_k(\theta)\,. \tag{13}$$

where

$$I_k(\theta) = \begin{cases} 1 : (k-1)\Delta\theta \le \theta < k\Delta\theta \\ 0 : otherwise \end{cases} \tag{14}$$

Generally, $G(\theta, f)$ is assumed a smooth continuous function with respect to the wave direction. This is mathematically expressed by the following relationship between three consecutive values of the estimate.

$$\sum_{k=1}^{K} (x_k - 2x_{k-1} + x_{k-2})^2 \approx 0\,. \tag{15}$$

The optimal estimate of $G(\theta, f)$ is obtained by maximizing the likelihood function with respect to x_k within the range where Eq. (15) does not become too large. These criteria can be formulated using an appropriate parameter u^2. The most suitable value of the hyper parameter u^2 and the estimate of σ^2 can be obtained by minimizing the Akaike Bayesian Information Criterion (ABIC) [Akaike, 1980] given by:

$$ABIC = -2ln \int L(x,\sigma^2) p(x|u^2,\sigma^2) dx \tag{16}$$

3. Data Collection

This research study was investigated with video camera observation from Hasaki beach in Japan. Source of data for this research was carried out by Port and Airport Research Institute (PARI), Japan [Suzuki and Yanagishima, 2009]. Since 1986, many coastal studies have been conducted in this location especially around the pier which is known as HORS (Hasaki Oceanographical Research Station). The Hasaki beach itself is located on 120 km east of Tokyo facing the North Pacific Ocean as shown in Fig. 1.

In Hasaki beach, bathymetric survey measurements were periodically conducted once or twice a year near HORS pier within area about 600 m alongshore direction and 700 m long in the cross-shore direction. For the map of bathymetry survey conducted on August 2006 is shown in Fig. 2. The HORS pier is located at $x = 0$ m where in-situ wave pressure gauges installed. The HORS pier has dimension about 427 m long with 3.3 m width of deck. The actual surface fluctuations in the Hasaki site were recorded using several ultrasonic wave gauges. The ultrasonic wave gauges were installed on the pier with position $x = 370$ m, $x = 230$ m, and $x = 145$ m from the shoreline. Water surface fluctuations were recorded as 60 minutes segment, each of which contains approximately 7200 data points, at a sampling rate of 2 Hz.

Meanwhile, image data were collected by using single camera installed in HORS pier at Hasaki beach, Japan in 2006. The digital video camera with the resolution of 640 x 420 pixels was used to acquire snapshot images. This video camera was mounted 10 m high above the ground level. The video image data was recorded for 15 minutes duration at every one hour interval with frequency sampling interval of 1 Hz.

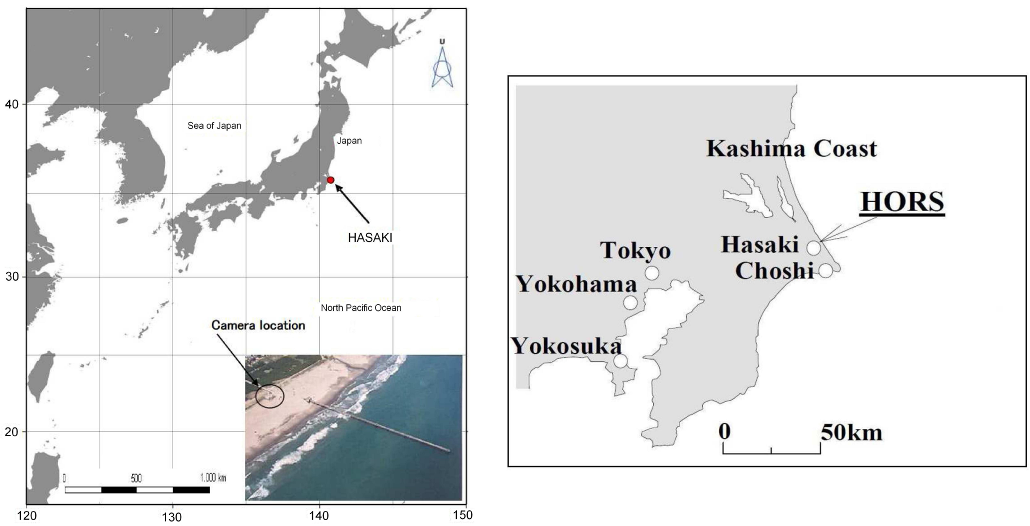

Fig. 1. Location of the study area.

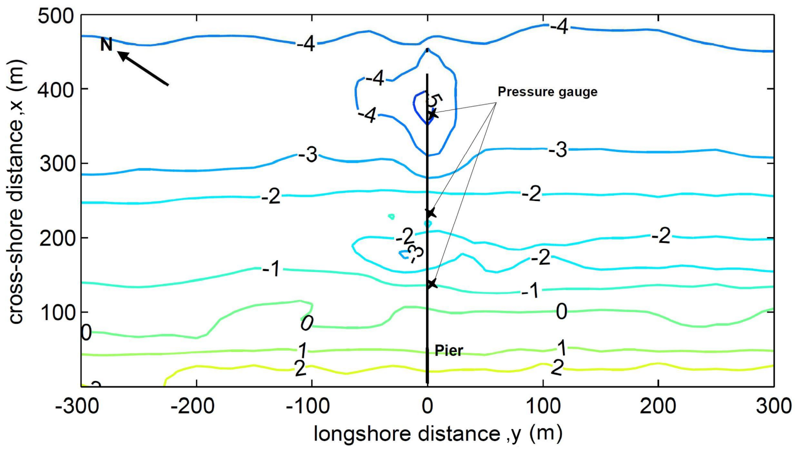

Fig. 2. Bathymetry contours from survey measurement conducted on August, 2006 at Hasaki pier. Pressure gauges mounted on pier at 145 m, 230 m, and 370 m from shoreline, respectively.

In 2006, the yearly average significant wave height $H_{1/3}$ is about 1.06 m with corresponding wave period $T_{1/3}$ is 8.4 sec based on the Nationwide Ocean Wave Information network for Port and HArborS (NOWPHAS) station at Kashima Port. During normal condition, waves approach the coast most often from the East and South East directions. However, the largest storm waves, with $H_{1/3}$ greater than 2-5 m, are incident from Northwest direction. The average of the tidal range is about 1.60 m.

4. Data Analysis

4.1. *Image view analysis*

Firstly, visual examination is done on all the existing images of the Hasaki beach which recorded from August 2006 until December 2006 to getting the right images. In order to study relationship between image and wave gauge data, it is important to remark that they were obtained in two different ways. The wave gauges data is represent as true water surface elevations. On the other hand, optical images data which represent the sea surface elevation dependent on wave slope and other phenomena such as sea ripples, wave breaking, sun glitter, etc [Populus *et al.*, 1991]. This issue, especially the influences of light reflection on sea surface from optical images or photographs to estimate directional spectra can be found in many literatures [e.g., Cox and Munk, 1956; Stillwell, 1969; Stillwell and Pilon, 1974].

From visual analysis, it is appear that wave height below 1.0 m (calm condition), the snapshot images have good quality image, and above 1.6 m wave height (moderate condition), very few good images are available. These are due to sea ripples from wave breaking. Meanwhile, due to increase of wave height and bad weather

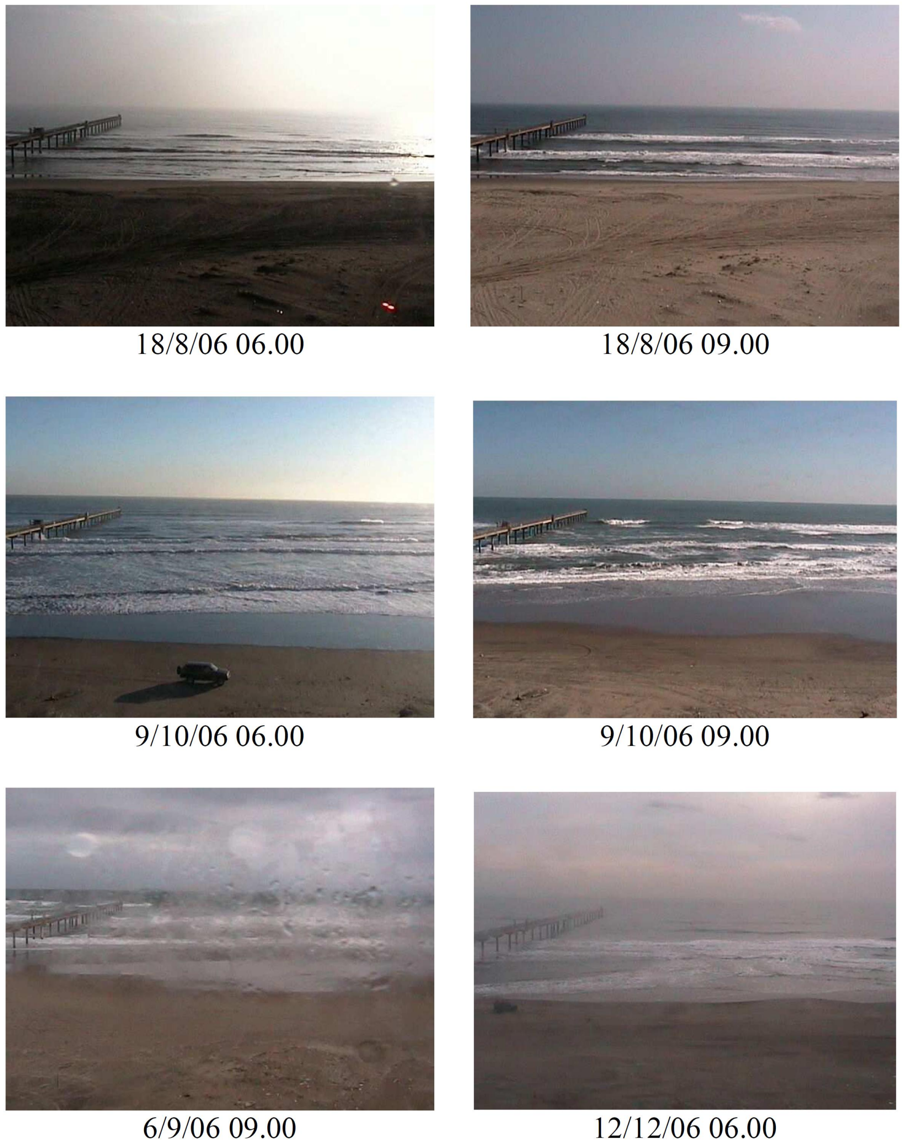

Fig. 3. Snapshot images at Hasaki pier. (Top) snapshot images on calm condition with wave coming from ESE during August. (Middle) snapshot images on moderate situation with wave direction coming from NNE during October and (Bottom) example of snapshot images on storm condition.

condition in storm condition, as expected, to get good images qualities is very difficult. Fig. 3 shows the examples of snapshot images at HORS pier for different conditions. The parameters which seem to influence the image quality are varying weather conditions (such as cloudy or rain), wave conditions and sun light.

4.2. *Rectification image analysis*

Before further analysis, in order to collect qualitative data, firstly, rectification of the image must be carried out in order to extract quantitative data from a sequence of snapshot images. Rectification involves photogrammetric transformations, which convert image coordinates $(u,\ v)$ into the real world coordinates $(x,\ y,\ z)$. This transformation was based on the standard photographic method as proposed and described in Holland *et al.* [1997]. Rectified images result from snapshot images are shown in Fig. 4 below.

The next procedure to analyze nearshore wave field with video images is to derived time series of pixel brightness on video images. From rectified images sequence as shown in Fig. 4, time series of pixel brightness intensity at specific point where the wave gauge is located then can be formed. Fig. 5 shows the examples of time series at $x = 230$ m (outside breaking area) from the wave gauge and pixel brightness on video images sequence which correspond to the nearest location of the wave gauge.

The time series of pixel brightness on video images may have introduced possible some source of error corresponding to the pixel resolution resulting from rectification procedure. Because the actual area occupied by a pixel in the image will increase with increasing distance from the camera. Figure 6 shows scale distortion result from rectification image. Accuracy of rectification analysis depends on camera distance and position. Therefore coastal video system must be mounted as high as possible in such a way that view angles of camera can be perpendicular to the water surface.

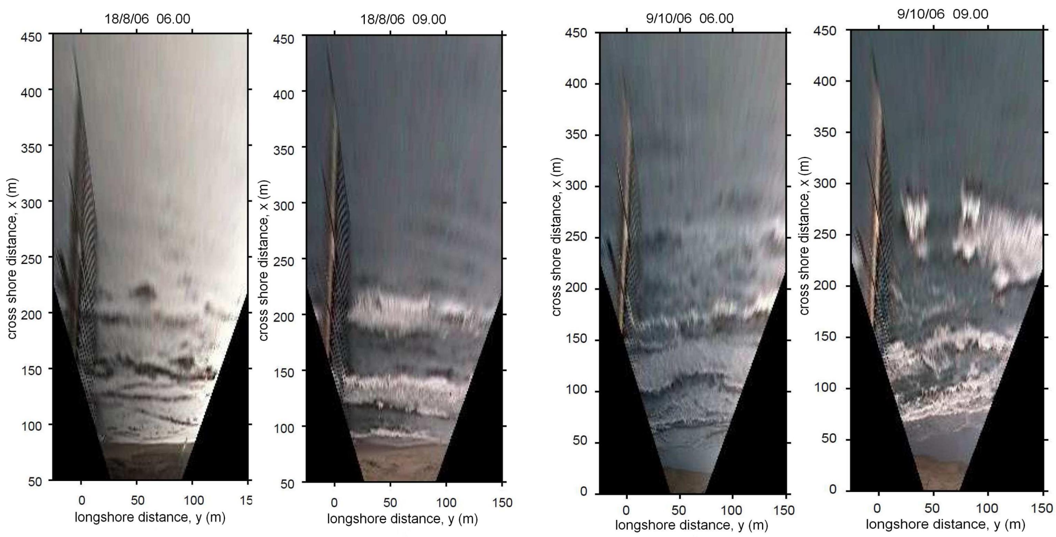

Fig. 4. Examples of rectified figures from snapshot images at Hasaki pier.

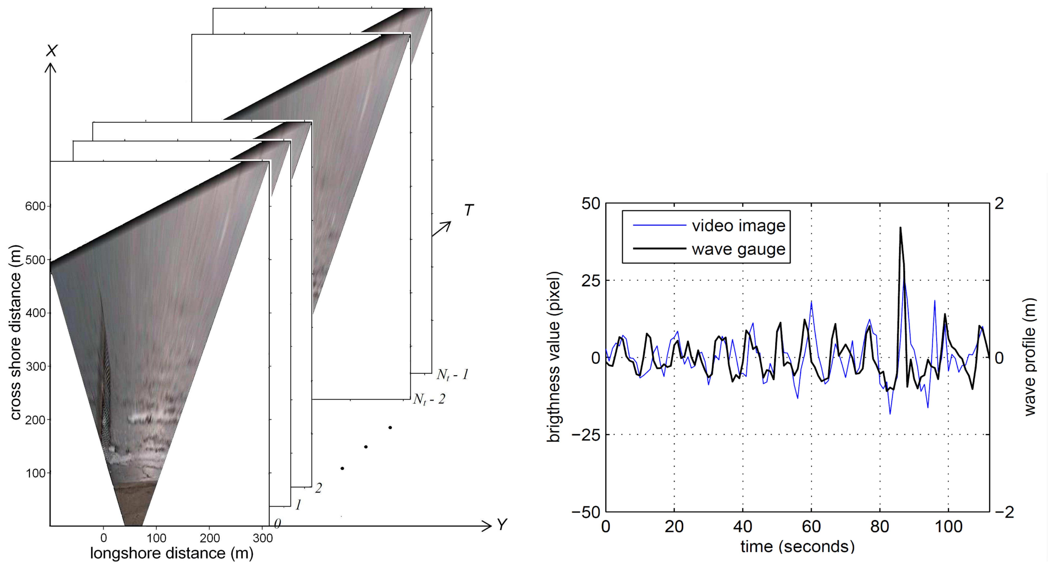

Fig. 5. Time series of rectified images results (left-a). Comparison time series of wave profile from a wave gauge with sampling frequency 0.5 Hz and pixel brightness on video images with sampling frequency 1.0 Hz (right-b).

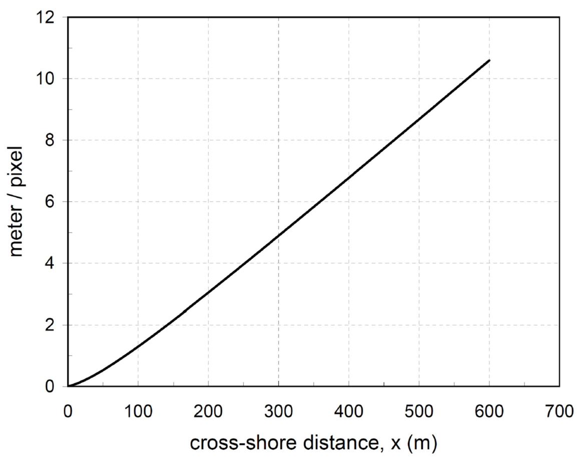

Fig. 6. Scale distortion result from rectification of snapshot image.

5. Results and Discussions

5.1. *Wave frequency spectrum*

In this work, video images recorded on 18 August 2006 were used in the spectral analysis. In this day, the observed significant waves height based on NOWPHAS data base was below 1.0 m and the wave direction was approach from NE direction.

Wave frequency spectra were calculated based on Fourier transform in combination with overlapped, segmented and averaging procedure as given in Bendat and Piersol [1986]. Due to the short time series used in the video images data (around 15 minutes), the time series of 512 points data were used in the analysis. Time series of 512 points sampled at 1.0 second were first standardized using zero mean and subdivided into 128-points segment with 50 % overlap for spectral estimation. This process of analysis resulted in 7 segments of data with spectral resolution of 0.0078 Hz. Fast Fourier Transform was implemented with each Hanning-window segment and averaged to calculate wave frequency spectrum. The results of wave spectrum of pixel brightness on video image are presented in Fig. 7.

Comparison of wave spectrum between time series of pixel brightness on video images and in-situ measurement is shown in Fig. 8. In order to make comparable, we have used their respective peak spectral densities for normalization, since the energies of the frequency spectra of the pixel values and wave profile measurements

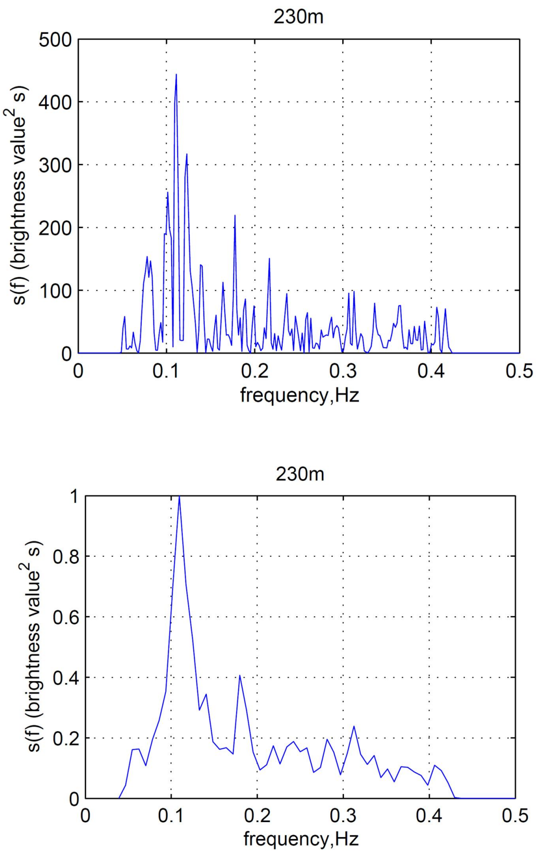

Fig. 7. Examples of raw spectrum (top) and smoothed spectrum (bottom) from pixel brightness on video images .

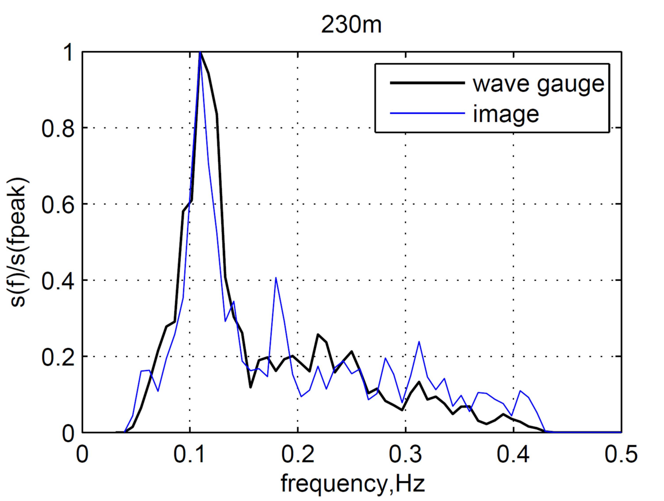

Fig. 8. Comparison of wave spectrum from video images and in-situ sensor recorded on 18 August 2006 at 09.00 h.

were measured in different scales. It can be seen that the normalized spectral are similar in shape. The figure shows narrow band spectrum with major sharp peak at frequency 0.117 Hz, which corresponds to peak period of 8.5 seconds. This peak frequency corresponds with peak period from offshore measurement ($T_{1/3} = 8.2$ seconds). Meanwhile multiple weaker peaks appear at higher frequency from 0.2 Hz to 0.4 Hz. These multiple weaker peaks are presence due to nonlinear wave component which is a typical characteristic of shallow water spectrum. Below 0.05 Hz and above 0.4 Hz, the white noise decreases due to band-pass filter with a high pass filter and a low pass filter.

Fig. 9 shows another example of comparison between the wave spectra from video images and in-situ measurement on 18 August 2006. In the figures, the peak frequency was very close in both wave spectra. While in some cases, for example at 11.00 h and 15.00 h, the video images and in-situ spectra presented different peak frequency. This variability is because the accuracy of wave spectrum from video images which represent the sea surface elevation dependent on viewing conditions. Another possibility is because the frequency resolution from video images data is less than that of the wave gauge.

However, in general, it can be concluded that the video images and in-situ spectra show similar form with the frequency peaks positioned very close to each other as indicated in Fig. 10. The figure shows the single peak frequency observed from video images and in-situ measurement varied between 0.09 Hz and 0.13 Hz. The average of peak frequency from video images and in-situ are 0.09 Hz and 0.10 Hz, respectively. The average of peak frequencies agreed well with a difference of only 0.01 Hz and the root-mean-square error of the differences between peak frequencies of wave spectra derived from video images and in-situ measurement is 0.02 Hz.

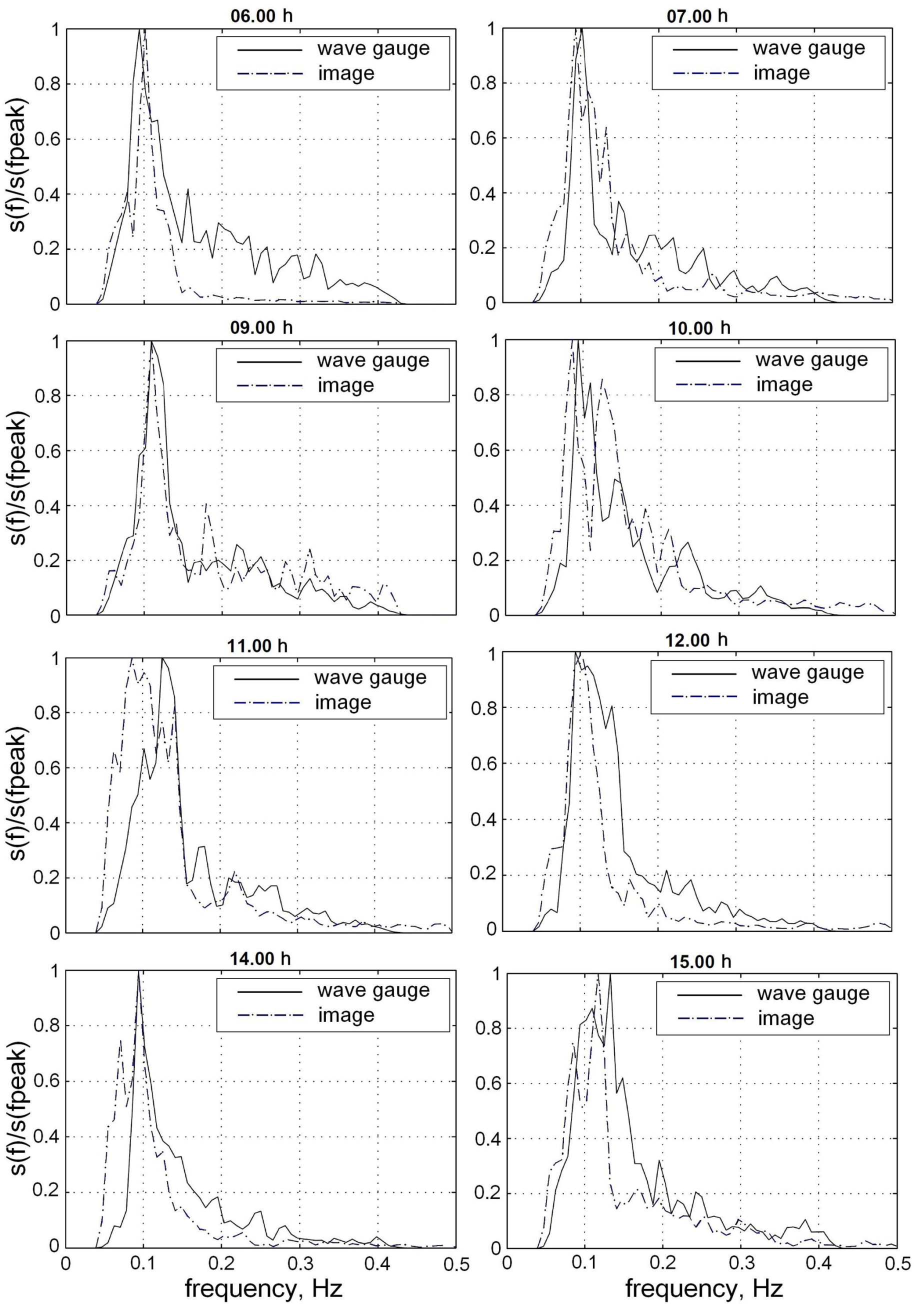

Fig. 9. Time series of wave frequency spectra estimated from video images and in-situ sensor on 18 August 2006.

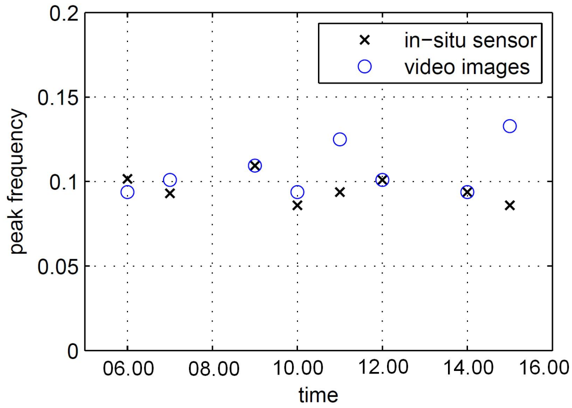

Fig. 10. Time series of peak frequency estimated from video images and in-situ sensor on 18 August 2006.

5.2. *Directional wave spectrum*

In this work, time series of pixel brightness on video images data is used to determine wave direction through directional wave spectrum. To determine wave spectrum directly from video images, a model of modulation transfer function is needed to connect the signals of video images with the wave field [Walker, 1994]. Because the complexity and non-linearity of transfer function between video images signal and the surface wave field are not well known, in this study, the assumption of a linear transfer function was applied to estimate the directional spectral from video images from Hasaki beach.

Estimation of directional spectral from video images has been based on Fourier transform method in time and both spatial dimensions using group of pixels brightness on video images data. Estimation of directional wave spectrum is based on the Extended Maximum Likelihood Method [Isobe, 1984] and the Bayesian Directional Method [Hashimoto, 1987]. In this work, the pixels can be considered equivalent to fixed instruments as wave probe sensor through use rectification process. High-resolution estimation of wave directional spectra require proper layout of pixels array at location of interest to minimize some errors in the cross-power spectra analysis. The important of the configuration of array to determine the directional spectra also reported by (among others) Young [1994], who investigated the performance of wave measuring system. Details on optimizing array layouts design can be seen on Goda [1985].

In this study, a star and polygon arrays design from brightness intensity of pixel data were used to estimate directional spectral at the distance 230-240 m from shoreline. The distance between pixels as optical instruments was set as $D/L = 0.2$, where L is the wavelength of the examined component wave. The dimension D is set to typical expected wavelength based on peak frequency and water depth on linear wave theory. For Hasaki site, D is design for wave period, $T= 8$ seconds in water depth of 2 meters. The wavelength would be approximately about 30-35 meters. With the distance between pixel D is 5 m, these wave are well resolved. The estimations of directional wave spectrum results are provided in Fig. 11 and Fig. 12, respectively.

First, the EMLM and BDM were applied to the case of a star array design for estimating directional wave spectrum of swell as shown in Fig. 11. The figure shows that both directional wave spectra shown clear peaks. The BDM result has directional spreading narrower compare to the EMLM with energy peak is higher than energy peak estimated by the EMLM. Also, energy leakage is present on directional spreading estimated by the EMLM. It is clearly shown that the accuracy of the directional spectrum estimate has been improved by using the BDM method. For mean direction estimation, Fig. 11 indicated that both methods estimate similar mean direction about 94 degree from shoreline which indicating the wave approach perpendicular to the shoreline.

Meanwhile, directional wave spectrum of swell calculated by the EMLM and BDM in the case of polygonal array design is presented in Fig. 12. Both methods yield similar mean direction within 86 degree at peak frequency 0.109 Hz. Directional spectrum of swell computed by the BDM has narrow directional function with more high energy peak compare to the EMLM. In addition, the BDM results from star and polygonal array systems had secondary sub-peaks at lower frequency. These

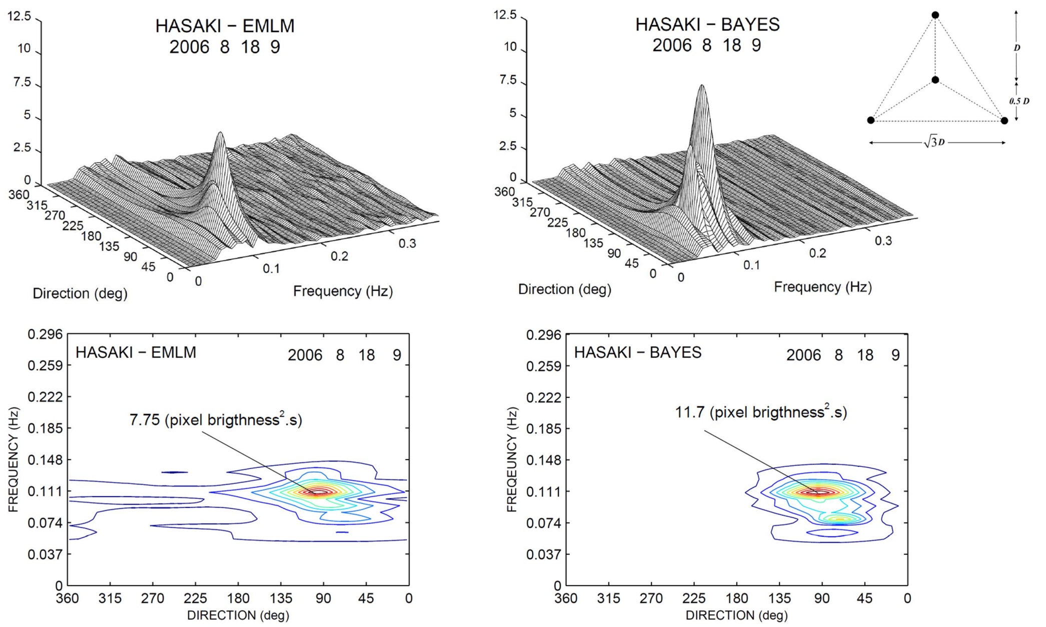

Fig. 11. Examples of the directional spectra for a star array estimated by the EMLM and BDM.

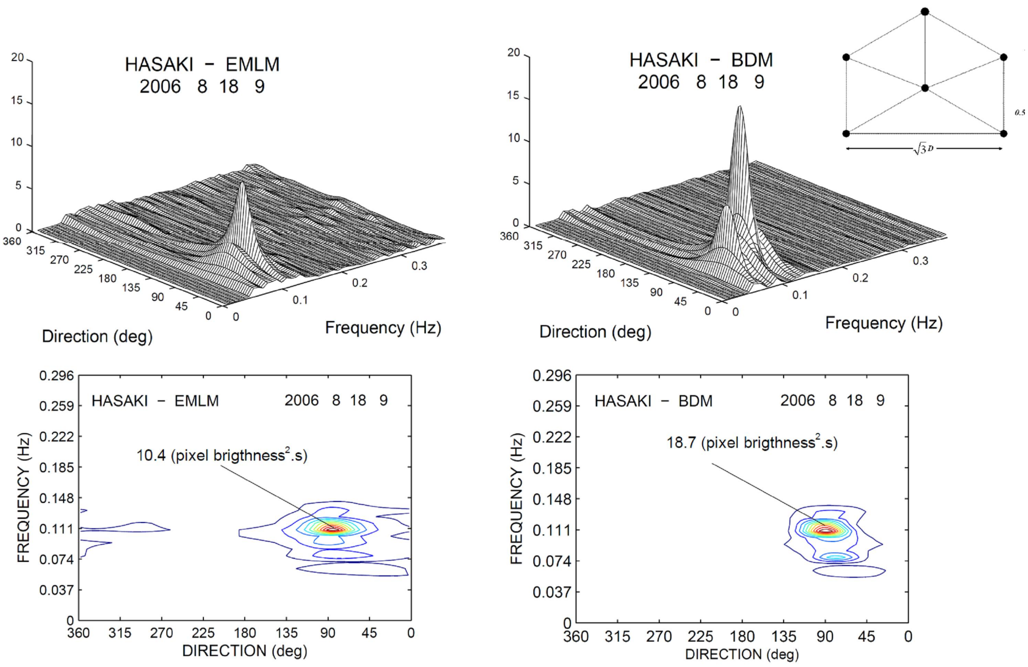

Fig. 12. Examples of the directional spectra for polygon array estimated by the EMLM and BDM.

sub-peaks appear may be due to the presence of long period wave oscillations near the shore as also reported by [Sundar *et al.*, 1999], who observed similar behavior analyzing nearshore of directional spectra.

Overall, both methods provide excellent directional spectra estimates for a star and polygonal array cases. The differences are that the directional wave spectra estimated by the BDM give higher spectral peak to the EMLM and yield similar shape of directional spectral estimate in case of a star and polygon arrays. Added, polygon array design provides narrow distribution function compare to star array design in both methods.

Finally, although the actual directional spectra are unknown, we suppose that the BDM method is accurate and efficient. The reason is due to the results of the numerical experiments carried out by Hashimoto and Kobune [1988] or Hashimoto [1987]. In their papers, the iterative computations of the BDM could minimize the errors in the cross-power spectra. Meanwhile, the EMLM can not adequately account for the error in the cross-power spectra, which strongly influence the stability of the estimate of directional spectrum. Also, the optimum estimates of directional spectrum from the BDM were shown to be almost identical to the true solutions with smooth and continuous directional spreading function [Hashimoto, 1987].

5.3. *Comparisons of directional wave spectrum retrieved from video images with numerical model*

Due to the lack of nearshore wave measurement data in shallow water wave, in this work, numerical model of SWAN has been selected to verify the results on directional wave spectrum from video images in shallow water. Because it is important to verify the results of directional spectrum from video images using whatever data are available [Zubier *et al.*, 2003] or even with different formulation such as using numerical model.

The model of SWAN is a third generation wave model developed at the Technical University of Delft in the Netherlands [Booij *et al.*, 1999] and it is open source or freely available. Specifically, SWAN wave modeling was developed for coastal and inland water zones. The model is based on the spectral action balance equation. The detail formulations of the SWAN code can be found in Booij et al., (1999) and Ris et al., (1999).

In this model, a rectilinear computation grid is used with a grid size of 5 m x 5 m. In order to minimize the effect of lateral boundaries, the computational domains were extended beyond area of interest as shown in Fig. 13. The computational grids extend for 900 m in the cross-shore direction. In the alongshore direction, the computational domains were extended on each side about 600 m. The input conditions for SWAN are defined along the offshore boundary of the rectangular domain at cross shore distance $y = 900$ m. Boundary conditions for SWAN computations used herein are taken from implementation results of the WAM model. Tidal measurements were also used to adjust the water depth in the SWAN computations.

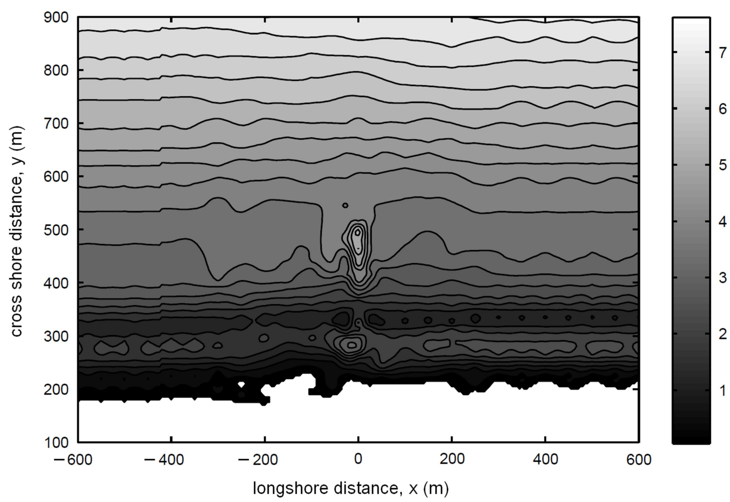

Fig. 13. Model domain and bathymetry for SWAN wave modeling

Before further analysis, the performance of SWAN computation was calibrated with data observations. The observed wave conditions located at the HORS pier (as indicated in Fig. 2) are compared to the SWAN output to calibrate the model. In this work, model has been simulated with default formulation with all the physical mechanisms such as wind generation, wave refraction, wave breaking, bottom friction, wave-wave interactions and white-chapping. An example of the significant wave height and wave direction results computed with SWAN is shown in Fig. 14. The figure shows for an incident wave height, $H_{1/3} = 1$ meter, period, $T_{1/3} = 8.0$ seconds and wave angle, $\theta = 101$ degree.

For comparison of significant wave height between SWAN model results and significant wave height on the wave gauge locations is presented in Fig. 15. The figure shows that SWAN simulates the significant wave height very well for two wave gauge locations (230 m and 370 m). In these two locations, the significant wave height computed by SWAN were closer to data observations but at other location (145 m), the significant wave height obtained by SWAN were smaller compare to in-situ wave gauge. Overall, the root-mean-square (rms) error of the differences between measured and estimated of significant wave height is 0.04 m.

The discrepancies results found on 145 m are due to the fact that in this location,

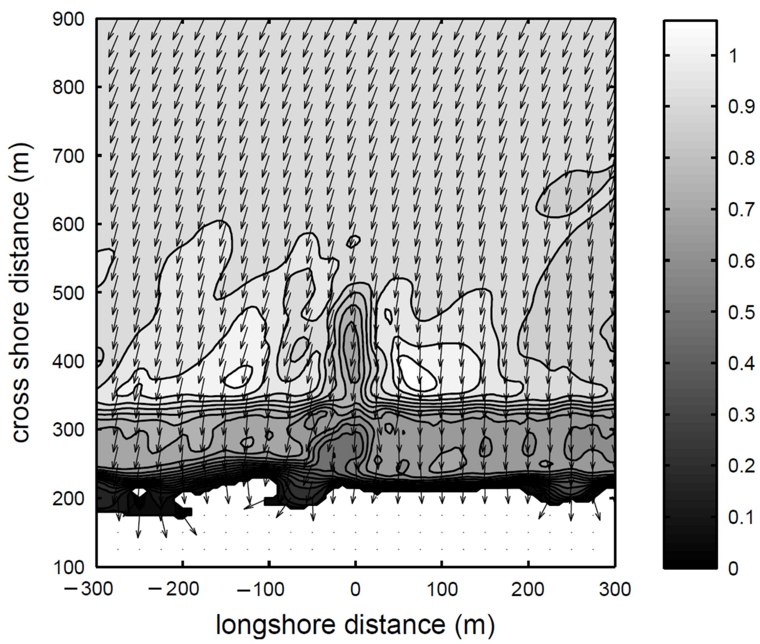

Fig. 14. Significant wave heights and wave directions computed by SWAN for 18 August 2006

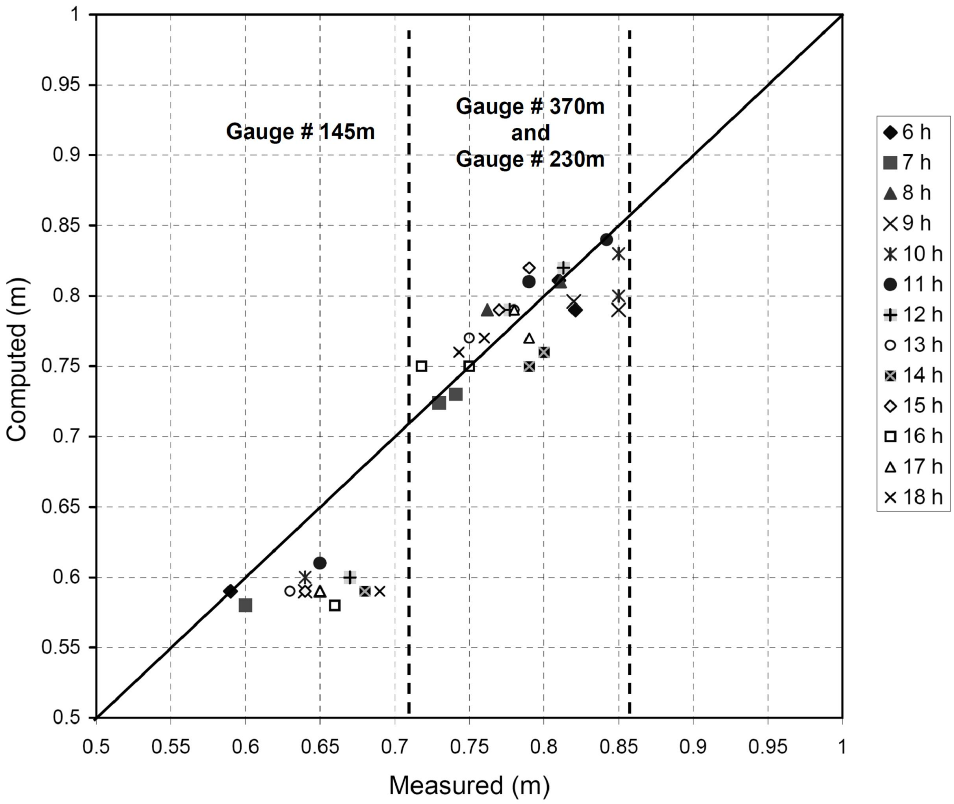

Fig. 15. Significant wave heights comparison for SWAN with data observations on 18 August 2006

the wave breaking occurs. The phenomena of wave breaking process are difficult to model through numerical model. Other possibility is that the data from wave gauges are significantly affected by wave breaking in this location.

In this study, we also examine frequency spectrum for three wave gauge locations, respectively. The results of frequency spectrum comparison between SWAN and data observations are presented in Fig. 16. In general, the frequency spectra results are similar with narrow band spectrum at peak frequency. In higher frequency, multiple weaker peaks appear for frequency spectra from field measurements. It is different with frequency spectra from SWAN, which indicated only a single secondary peak in higher frequency. Overall, the results of frequency spectra from SWAN are consistent with observations where the results indicated that transfer energy from to higher frequency when the waves approach to the shore.

After the model well calibrated, directional spectrum in shallow water can be generated as shown in Fig. 17 above. Fig. 17 shows directional wave spectrum generated from SWAN model at cross shore location 230-240 m from shoreline. For

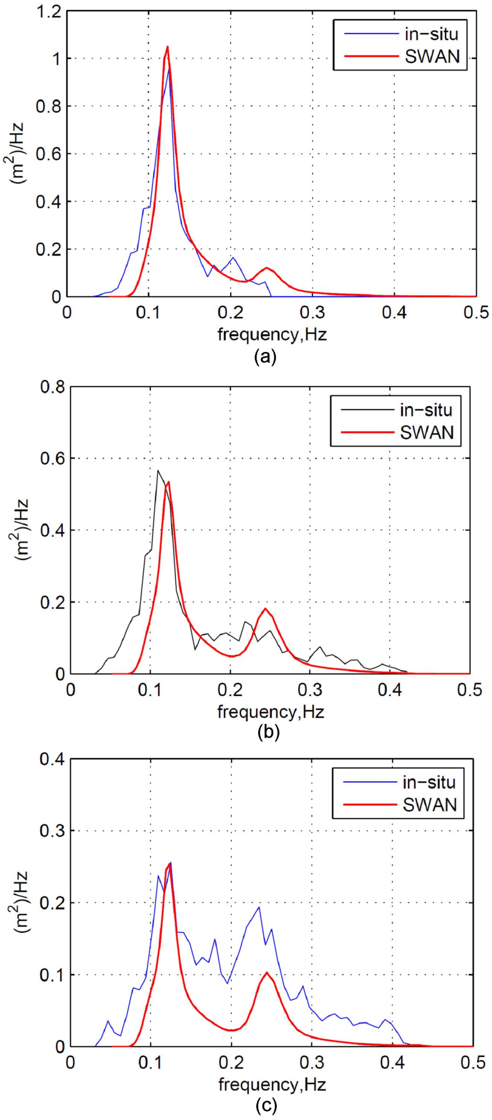

Fig. 16. Frequencies spectra obtained using SWAN and data observation at three wave gauge locations, respectively. (a) 370 m, (b) 230 m and (c) 145 m

comparison directional spectrum, the results show that there is a good agreement between directional wave spectra in shallow water estimated by SWAN and video images data. Both methods indicated that directional spectrum is significantly narrower in frequency and direction which is typical of swell waves as indicated in Fig. 17 and Fig. 18.

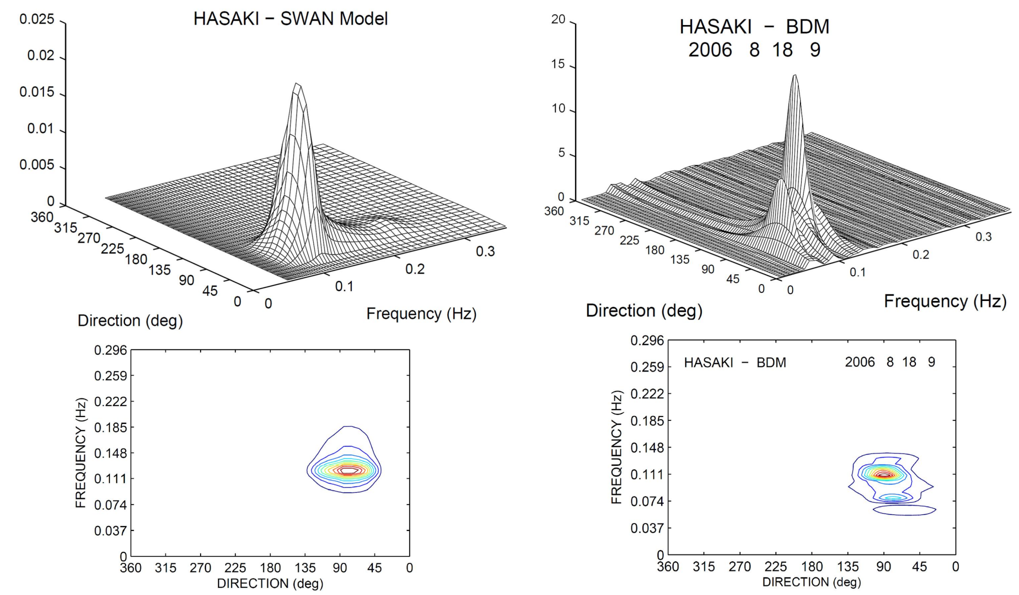

Fig. 17. Directional wave spectrum of swell on 18 August 2006 at 09.00 h from SWAN (left) and from video images (right)

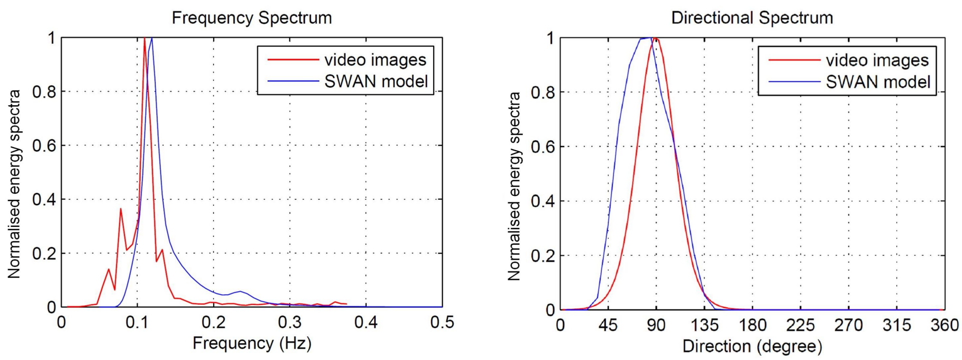

Fig. 18. Normalized frequency spectrum and directional spreading of swell from SWAN model (thin line) and from array of pixel brightness on video images (bold line)

6. Conclusions

The applicability of video images technique to derive directional wave spectrum using group of pixel brightness on video images have been presented. Samples time series of video images data at Hasaki beach in Ibaraki prefecture, Japan was used in this research. It was found that the peak frequencies estimated from pixel brightness on video images well correspond with the signal of in-situ measurement. This study also indicated that both methods (the EMLM and BDM) can successfully estimate directional wave spectrum in shallow water waves. It appears that the BDM provide more suitable and robust results than the MLM with the narrowest at peak frequency and direction.

Also, directional wave spectrum in shallow water area retrieved from video images data have been verified with spectral wave model of SWAN. Our model results demonstrated that SWAN model well calibrated with data observations to simulate wave fields around HORS pier in Hasaki beach. In the shallow water, directional wave spectrum generated with SWAN model was narrower at peak frequency and direction which is similar with directional wave spectrum derived from video images. Although the results have some uncertainties due to the limitations on the video images technique, as do all measurement methods, it is shown that video images method can be very useful to practical engineers considering shallow water wave conditions.

Acknowledgments

The authors wish to thank Port and Airport Research Institute (PARI), Japan for their data support during this study. Personally, I would also like to acknowledge funding provide by *Departemen Pendidikan Tinggi Indonesia* (DIKTI), *Institut Teknologi Sepuluh Nopember* (ITS), Surabaya, Indonesia and Kyushu University, Japan for financial support during our study.

References

Akaike, H. [1980] "Likelihood and Bayes procedure," in *Bayesian Statistics*, University Press, Valencia, pp. 143–166.

Aarninkhof & Holman, R. A. [1999] "Monitoring the nearshore with video," *Backscatter*, Vol. 10(2), pp. 8–11.

Bendat, T. S. & Piersol, A. G. [1986] *Random Data: Analysis and Measurement Techniques* (John Wiley & Sons, Inc., New York).

Booij, N., Ris, R. C. & Holthuijsen, L. H. [1999] "A third-generation wave model for coastal regions, 1, model description and validation," *Journal of Geophysical Research*, Vol. 104 (C4), pp. 7649–7666.

Cox, C. and Munk, W. [1956] "Slope of the sea surface deducted from photographs of sun glitter," *Bulletin of the Scripps Intitution of Oceanography*, Vol. 6, No. 9, pp. 401–488.

Chou, C., R., Yim, J.,Z., and Huang, W.,P. [2004] "Determining the hydrographic parameters of the surface of water from the image sequences of a CCD camera," *Experiments in Fluids*, Vol. 36, No. 4, pp. 515–527.

Davidson, M., Koningsveld, M. V., de Kruif, A., Rawson, J., Holman, R., Lamberti, A., Medina, R., Kroon, A. & Aarninkhof, S. [2007] "The CoastView project: developing video-derived Coastal Site Indicators in support of coastal zone management," *Coastal Engineering*, Vol. 54, pp. 463–475.

Goda, Y. [1985] *Random Seas and Design of Maritime Structure* (University of Tokyo Press), p. 323.

Hashimoto, N. [1987] "Analysis of the directional wave spectrum from field data," in *Advances in*

Coastal and Ocean Engineering, ed. Philip L. F Liu (World Scientific Publishing Co.Ptc. Ltd., Singapore), pp. 103–143.

Hashimoto, N. & Kobune, K. [1988] "Directional spectrum estimation from a Bayesian approach," *Proc. of 21st ICCE, ASCE*, pp. 62–76.

Hashimoto, N. & Tokuda, M. [1999] "A Bayesian approach for estimating of directional wave spectra with HF radar," *Coastal Engineering Journal*, Vol. 41(2), pp. 137–149.

Hasan, M, J. & Takewaka, S. [2007] "Obesrvation of a stormy wave field with X-Band radar and its linear aspects," *Coastal Engineering Journal*, Vol. 49(2), pp. 149–171.

Holman. & Chickadel, C. [2004]. "Optical remote sensing estimates of the incident wave angle field during NCEX," *Proc. of 29th ICCE, ASCE*, pp. 1072–1081.

Holman, R. A. & Stanley, J. [2007] "The History, Capabilities and Future of Argus," *Coastal Engineering*, Vol. 54, pp. 477–491.

Holland, K. T. & Holman, R. A. [1997] "Video estimation of foreshore topography using trinocular stereo," *Journal of Coastal Research*, Vol. 13(1), pp. 81–87.

Holland, K. T., Holman, R. A., Lipmann, T. C., Stanley, J. & Plant, N. [1997] "Video estimation of foreshore topography using trinocular stereo," *IEEE Journal of Ocean Engineering*, Vol. 22(1).

Isobe, M., K. Kondo, and K. Horikawa. [1984] "Extension of MLM for estimating directional wave spectrum," in *Proc. Symp. on Description and Modeling of Directional Seas*, Paper No. A-6, pp. 57–100.

Izquierdo, P., Nieto Borge, J. C., Geudes Soarez, C., Sanz Gonzalez, R. & Rodrigues, G. R. [2005] "Comparison of wave spectra from nautical radar images and scalar buoy data," *Journal of Waterway, Port, Coastal and Ocean Engineering*, ASCE, Vol. 131, pp. 123–131.

Krogstad, H. E. & Barstow, S. F. [1999] "Satellite wave measurement for coastal engineering applications," *Coastal Engineering*, Vol. 37(3-4), pp. 283–307.

Lippmann, T. C. & Holman, R. A. [1989] "Quantification of sand bar morphology: A video technique based on wave dissipation," *Journal of Geophysical Research*, Vol. 94(C1), pp. 885–1011.

Mitsuyasu, H., Tasai, F., Suhara, T., Mizuno, S., Ohkusu, M., Honda, T. & Rikiishi, K. [1975] "Observation of the directional spectrum of ocean wave using a cloverleaf buoy," *Journal Physical Oceanography*, Vol. 5, pp. 750–760.

Populus, J., Aristaghes, C., Jonsonn, L., Agustin, J. M. & Pouliquen, E. [1991] "The use of SPOT data for wave analysis," *Remote Sensing Environment*, Vol. 36 (1), pp. 55–65.

Plant, N. G. & Holman, R. A. [1997] "Intertidal beach profile estimation using video images," *Marine Geology*, Vol. 140, pp. 1–24.

Plant, N. G., K. T. Holland, & M. C. Haller. [2007] "Ocean wave number estimation from wave-resolving time series imagery," *IEEE Transactions on Geosciences and Remote Sensing*, Vol. 46 (9), pp. 2644–2658.

Ris, R. C., Booij, N. & Holthuijsen, L. H. [1999] "A third-generation wave model for coastal regions, 2, Verification," *Journal of Geophysical Research*, Vol. 104 (C4), pp. 7667–7681.

Stillwell, D.[1969] "Directional enegy spectra of the sea from photographs," *Journal of Geophysical Research*, Vol. 74, No. 8, pp. 1974–1986.

Stillwell, D., Jr. and Pilon, R. O. [1974] "Directional spectra of surface waves from photographs," *Journal of Geophysical Research*, Vol. 79, No. 9, pp. 1277–1283.

Sundar, V. & Sannasiraj, S. A, and Kaldenhoff, H. [1999] "Directional spreading of wave in the nearshore zone," *Ocean Engineering*, Vol. 26, pp. 161–188.

Stockdon, H. F. & Holman, R. A. [2000] "Estimation of wave phase speed and nearshore bathymetry from video imagery," *Journal of Geophysical Research*, Vol. 105, pp. 22015–22033.

Suzuki, K and Yanagishima, S. [2009] "Observation of nearshore processes using network camera," *Proceeding of Coastal Dynamics 2009*, Paper No. 115, 10p.

Walker, R. E. [1994] *Marine Light Field Statistics* (John Wiley and Sons, Inc, New York), 675p.

Young, I. R. [1994] "On the measurement of directional wave spectra," *Aplied Ocean Research*, Vol. 16, pp. 283–294.

Zikra, M., Yamashiro, M., Hashimoto, N. & Suzuki, K. [2010] "Bathymetry inversion using video image in shallow water," *Annual Journal of Civil Engineering in the Ocean*, JSCE, Vol. 26, pp. 1161–1166.

Zikra, M., Hashimoto, N., Yamashiro, M. & Suzuki, K. [2011] "Spectral analysis of pixel brightness on video images to study wave analysis at Hasaki beach in Japan," *CD Rom Proceeding of 21st International Offshore and Polar Engineering Conference*, ISOPE, pp. 974–979.

Zubier., K., Panchang., V. & Demirbilek., Z. [2003] "Simulation of waves at Duck (North Carolina) using two numerical models," *Coastal Engineering Journal*, Vol. 45 (3), pp. 439–469.